Research Article

High Temperature Vacuum Annealing and Hydrogenation Modification of Exfoliated Graphite Nanoplatelets

Xiaobing Li,[1,2] Sanjib Biswas,[1,3] and Lawrence T. Drzal[1]

[1] *The Composite Materials and Structures Center, Department of Chemical Engineering and Materials Science, Michigan State University, 2100 Engineering Building, East Lansing, MI 48824, USA*
[2] *Department of Civil Engineering, University of Mississippi, 106 Carrier Hall, University, MS 38677, USA*
[3] *Engineering and Process Science, The Dow Chemical Company, Midland, MI 48674, USA*

Correspondence should be addressed to Lawrence T. Drzal; drzal@egr.msu.edu

Highly active defect sites on the edges of graphene automatically capture oxygen from air to form various oxygen groups. A two-step procedure to remove various oxygen functional groups from the defect sites of exfoliated graphene nanoplatelets (GNPs) has been developed to reduce the atomic oxygen concentration from 9.5% to 4.8%. This two-step approach involves high temperature vacuum annealing followed by hydrogenation to protect the reduced edge carbon atoms from recombining with the atmospheric oxygen. The reduced GNPs exhibit decreased surface resistance and graphitic potential-dependent capacitance characteristics compared to the complex potential-dependent capacitance characteristics exhibited by the unreduced GNPs as a result of the removal of the oxygen functional groups present primarily at the edges. These reduced GNPs also exhibit high electrochemical cyclic stability for electrochemical energy storage applications.

1. Introduction

Graphene can be considered a polycyclic aromatic hydrocarbon [1–4]. The basal plane consists of sp^2-hybridized carbon atoms in a honeycomb lattice structure [1–4]. However, the size of the basal plane of graphene is finite, and some of the carbon atoms in the highly aromatic basal plane terminate at the edges in a nonaromatic state. The carbon atoms present at the edges are highly chemically active as compared to the chemically inert carbon atoms present in the basal plane [5, 6]. During the preparation of graphene nanosheets, the edge carbon atoms can react spontaneously with atmospheric oxygen to create carboxyl, keto, or hydroxyl group [5–7].

GNPs developed by the Drzal research group in Michigan State University are prepared by acid intercalation and rapid exfoliation process in a microwave environment. The acid-intercalated graphite particles undergo substantial expansion to form worm-like products, which are then mechanically grounded to generate small stacks of graphenes that are 1 to 15 nanometers thick, with diameters ranging from submicrometer to 100 micrometers. The size of the resulting GNPs can be further reduced to a few hundred nanometers by vibratory ball milling over extended period of a few days. The exfoliation process and morphologies of GNPs are detailed elsewhere [7]. The exfoliation process minimizes the presence of basal plane defects so that the number of edge sites is fixed for a given platelet size. Surface analysis indicates a proportional increase in the atomic oxygen concentration with decreasing graphene nanosheets dimension [8, 9]. For large GNPs with an average lateral dimension 15 μm and surface area around 270 m^2/g, the oxygen atomic concentration is less than 5% [8, 9]. However, for small GNPs with an average dimension less than 500 nm and surface area close to 550 m^2/g, the oxygen atomic concentration increases to about 10% [8, 9]. The edge chemical composition is important for dispersion in various media as well as for electron transport between graphene nanosheets when they are dispersed in polymers or used by themselves in bulk applications.

Application of GNPs of variable sizes for enhanced super-capacitor electrode performance was presented earlier [8, 9].

It was shown that the incorporation of large GNPs enhanced the electronic charge transport within the bulk macroscopic configuration for high power supercapacitor electrode applications [8, 9]. However, the hydrophobicity of the large area aromatic basal plane often restricts the wetting and dispersion of the aqueous-based electrolytes inside the bulk electrode. It has been demonstrated earlier that the incorporation of smaller GNPs with higher edge oxygen content relative to the basal plane area provides better wettability of the electrode to facilitate ionic electrolyte transport [8]. The increase in the specific capacitance can be attributed to increased specific surface area and the presence of oxygen functional groups at the nanosheet edges. The presence of oxygen functional groups significantly enhances the specific capacitance from the change in the oxidation states at different applied electrode potentials [10, 11]. At the same time, the changing potential can cause the reversible transformation of different oxidation states of the surface functional groups to alter the potential capacitance relation significantly [10–13]. In comparison to the large aromatic basal plane area in larger GNPs, the smaller nanosheets are therefore expected to exhibit a complex potential capacitance relation due to the presence of highly surface active oxygen content [12, 13]. The complex potential capacitance relationship also affects the performance of electrodes for electrochemical capacitor applications. The increasing edge chemical functionalities introduce a series of contact resistances over the large microscopic areas causing a significant voltage drop during the discharge of the capacitors at high current densities.

Therefore, it is worth of investigating the removal of oxygen groups on GNPs. But the removal of oxygen from the edge defect sites is completely different from that for removal of oxygen on the basal plane, which has been extensively studied earlier in the reduction of graphite oxide (GO) [3, 14–16]. Few results have been published specifically addressing the reduction of oxygen on the edges of graphene nanosheets. Chemical approaches are useful to reduce oxygen functionalities and convert GO back to graphene using hydrazine [14–16], sodium borohydride ($NaBH_4$) [17], and hydroquinone [18]. Simple high temperature annealing of GO has also been reported [14]. GO was also exfoliated and reduced by rapid heating to high temperature (up to 1050°C) to produce graphene nanosheets [19]. However, all of these approaches still leave residual oxygen content of about 8 atomic% or higher. The residual oxygen is likely concentrated on the defect sites. Also, simple thermal annealing of GO at temperatures of 1000 to 1100°C [14, 20] could only produce graphene with ~7 atomic% of oxygen, and the resulting reduced GO exhibits electronic properties inferior to pristine graphene [14] as suggested by Park and Ruoff [19].

The reduction of oxygen on graphenes has been extensively focused on GO wherein the improvement in conductivity is due to the increased fraction of sp^2 carbon atoms after the reduction treatment. These carbon atoms are on the basal plane, and the enhanced electrical conductivity is mainly within individual graphene sheets [14]. Alternatively graphene nanosheets of 3–5 nm thicknesses can be produced

by nonreactive approaches, such as microwave-assisted exfoliation of acid-intercalated graphite or ball milling of natural graphite [19], wherein the harsh oxidation reaction responsible for the generation of basal plane defects is avoided. However, oxygen functional groups are always detected because defect sites inevitably exist on the edges. Even the as-received graphite contains a few percent of oxygen. Little information can be found on the removal of O-groups from the edges of graphene nanosheets. Treatment of pristine graphene nanosheets with hydrazine and hydroquinone under various conditions in our laboratory did not show any result of reduction. Akhavan [20] thermally annealed GO, but analysis showed that the surface still retained 7 atomic% of oxygen. Most likely this is a result of the reaction of active carbon edge sites with the atmospheric oxygen to regenerate the oxygen functional groups at the edges. Therefore, it is crucial to passivate the edge carbon atoms to reduce the oxygen content at the defect sites of graphene nanosheets.

In this study, we report a two-step process in which submicron GNPs were vacuum-annealed at high temperature (550°C) to remove oxygen groups from the defect sites, and then the defect sites were capped with hydrogen atoms in the temperature range of 100–250°C to prevent the rapid graft of oxygen groups converted from oxygen source in air upon exposure to normal ambient environment. The hydrogen atoms came from the dissociation of H_2 in a mixture of argon (97 vol%) and hydrogen (3 vol%) under 800°C. The electronic properties of the treated graphene nanosheets were investigated.

2. Experimental

2.1. Materials and Methods. GNPs of about 500 nm, surface area of 510–540 m^2/g were prepared from microwave-assisted exfoliation of acid-intercalated graphite and size-reducing ball milling in which the slurry of exfoliated GNPs/isopropanol and milling balls were vigorously vibrated in a sealed steel container for few days. The simple annealing experiments took place in the quartz tube (inner diameter: ~8 mm) reactor described in Figure 1. The process began with a pump/purge cycle using argon to remove any residual oxygen. Next, the reactor was evacuated to a pressure of less than 2.7 Pa, and the temperature was raised to 550 ± 5°C and for 30 min. After vacuum annealing, the tube was flushed with Ar, cooled to room temperature, sealed (via V2) and then transferred in an argon glove box (oxygen below 20 ppm, H_2O below 2 ppm). Two XPS samples were prepared from the annealed GNPs. The first one was transferred under Ar atmosphere, and the second was exposed to air prior to loading into the XPS chamber.

The vacuum annealing and hydrogenation were carried out in a 20 mm diameter quartz reactor as shown in Figure 2. Prior to the experiment, the temperature profile along the axial direction of the tube reactor was mapped under the conditions of 550–600 mL/min H_2 (3 vol%)/argon flow rate and the temperature of 800°C to determine where the GNPs were to be placed. After the sample was loaded, the system was sealed to outside air and flushed. Then, V2 and V4 were closed as shown in Figure 2(b). All the rest valves were open.
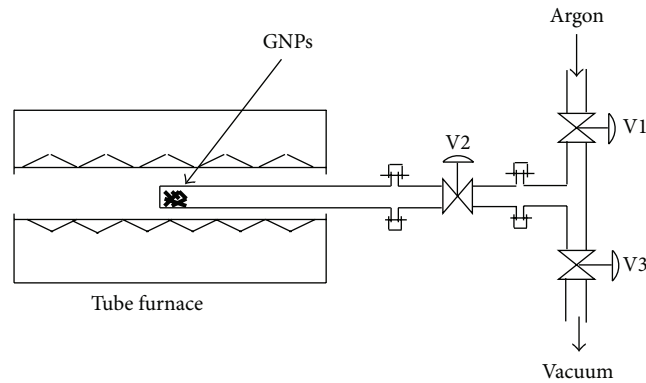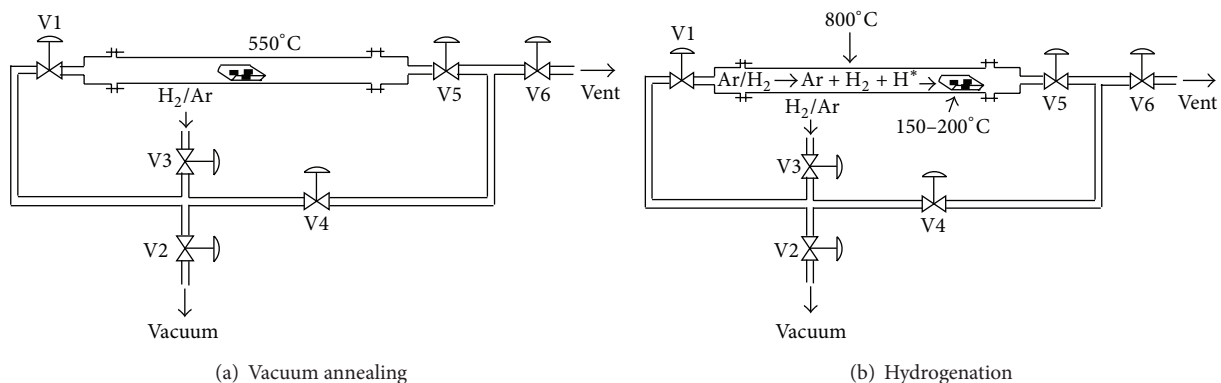
Figure 1: Direct vacuum annealing of GNPs.

(a) Vacuum annealing

(b) Hydrogenation

Figure 2: Two-step treatment of GNPs.

The system was flushed with the same H_2/Ar mixture to remove residual oxygen. Next, the reactor was evacuated, and the center of the tube reactor was heated to 550°C and kept isothermal for 30 min.

After annealing, the sealed tube was tilted slightly to allow the graphene to move to the cooler region of the reactor, where temperature could be about 200°C. The temperature at the center was increased to 800°C while keeping the $H_2/argon$ flow rate at 550–600 mL/min. Hydrogenation was carried out in two steps, first at 200°C for 1 hr followed by another 1 hr at 150°C. For hydrogenation at about 150°C, the quartz boat with the graphene nanosheets was moved closer to the end of the tube reactor. Finally, heating was stopped, and the system was cooled to room temperature to remove the treated sample for characterizations.

The surface resistance of the film was measured using a standard four-point probe measurement from Keithley 2400 source meter. Graphene nanosheets were dispersed in isopropanol assisted by small tip sonication for 1-2 min to form slurry of graphene nanosheets/isopropanol. The specimens were prepared by spray coating of slurry of nanosheets/isopropanol on a rectangular glass substrate. Three different locations were chosen for each sample in the test.

2.2. Instrument. The thermogravimetric analyzer (TGA), Q50 from TA Instruments, New Castle, DE, USA, was used to determine the weight loss for both the reduced and the unreduced samples. The analysis was carried out at 5°C/min heating rate in air.

In the Raman spectroscopy characterization, a Horiba Jobin Yvon LabRAM Aramis Raman Spectrometer with a 532 nm laser was used. The laser diameter used in our experiment was 10 μm, which was large enough to include the edges of 500 nm graphene nanosheets within the bulk sample to exhibit a pronounced disorder or defect induced D-band peak near 1340 cm^{-1} wavelength. Eight different locations were selected in the test.

The X-ray photoelectron spectroscopy (XPS) analysis was carried out with a magnesium K α X-ray source in Perkin Elmer Phi 5400 ESCA system at pressure between 1.33×10^{-6} and 1.33×10^{-5} Pa with pass energy of 29.35 eV and a take-off angle of 45°.

2.3. Potential Capacitance Analysis. The potential capacitance analysis was carried out in a two electrode configuration with the area and loading of the active electrode materials in the counter electrode kept much higher than working electrode for the measurement. A 0.1 M NaF aqueous solution was used for all the potential capacitance analysis. For electrochemical stability analysis, the two electrode configuration was used with equivalent loading of active material on both electrodes. The loading of GNPs was close to 4 mg/cm^2.

3. Results and Discussion

Since exceptionally high temperature may damage graphene samples and too low temperature may not be sufficient to remove oxygen groups at the defect sites, we vacuum (2.7 Pa) annealed GNPs at 550°C referring to the work of Ihm et al. [21], in which carbon nanotubes were annealed at 500°C under high-vacuum (2.7×10^{-5} Pa) for 30 min to remove oxygen completely.

The condition for hydrogenation is important as well. Dinger et al. [22] found that CH armchair groups and CH zigzag groups on the edge of graphite layer decomposed at 327°C and 377°C, respectively. Therefore, hydrogenation of graphene nanosheets only occurs in a certain temperature range which we found to be 100–250°C, and this is consistent with the above published results. In this study, the heat treated sample was hydrogenated for 1 hr at 200°C and 1 hr at 150°C, respectively.

In order to prove the need to passivate edge carbons with hydrogen, a simple annealing of the GNPs was performed. After vacuum annealing of GNPs, half of the sample was transferred to a stainless steel vessel in an argon glove box in which oxygen was kept below 20 ppm. A sealed transfer vessel was used to move the sample to an XPS system without exposure to the air. The other half of the treated sample was exposed to air under room temperature for 24 hrs before XPS analysis. A vacuum heat treated and hydrogenated sample (GNP-H) was also analyzed by XPS. Figure 3 displays the overall XPS scan of GNPs treated in different stage indicating relative concentrations of elements in each sample. The data in Table 1 shows that vacuum annealing at 550°C for 30 min can reduce oxygen to a very low level of 2.1 atomic%. However, after exposure to air even under ambient conditions, the oxygen level increased close to its original level. The annealing followed by the hydrogenation and then exposure to the atmosphere resulted in a reduction of surface oxygen content by ~50% to 4.78 atomic% of oxygen concentration. The limitation in further reduction in oxygen might be the result of physical events. The outermost GNPs had full access to the reducing and hydrogenation environment, but not all of the GNPs in the bulk graphene stack were sufficiently exposed to the reducing atmosphere during the experiment, as shown in Figure 4.

The deconvolution of C1s XPS signal provides important information on the changes in the carbon molecular state. Mattevi et al. [14] reported the thermal annealing of GO in vacuum or in argon/H_2 atmosphere in the temperature range of 500–600°C to effectively increase the sp^2 fraction by reducing the sp^3 content after the removal of oxygen functional groups. The deconvolution of the C1s peak showed carbon in six different chemical bond environments: C=C/C–C aromatic ring at 284.6 eV; the asymmetrical envelope corresponding to damaged alternate hydrocarbon with sp^3 radical near ~285.4 eV; the carbonyl group C–O at 286.1 eV; the keto C=O at 287.5 eV; the carboxylic acid group O=C–OH at 289.2 eV; and a broad π-π^* near 290.6 to 291.4 eV [14, 23, 24]. However, annealing above 600°C resulted in only a slight increase in graphitic carbon [14]. Similar analyses of carbon-carbon and carbon-oxygen bonds were reported for GO

Table 1: Oxygen concentrations of graphene nanosheets after treatment.

Sample	Oxygen conc. (atomic%)
GNP	9.49
GNP annealed without exposure to air	2.14
GNP annealed then exposed to air	7.97
GNP-H	4.78

reduced by $NaBH_4$ [17]. The C1s regions for the above three treated samples in our experiment revealed the molecular nature of carbon and C–O bonds as seen Figure 5 and in Table 2. The C/O atomic ratio for the unreduced sample was 12.7 but increases to 23.2 for the reduced sample indicating the reduction of various oxygen functional groups. The peak intensity analysis gives a clear indication of the reduction of oxygen functional group containing carbon atoms to sp^3 and sp^2 hybridized C–H bonds. The increase in the sp^2 content of the sample with the increase in the intensity ratio of the aromatic C=C/C–C peak at 284.6 eV relative to the damaged alternate C–H bonded sp^3 peak near 285.5 eV for the reduced sample reveals the successful conversion of sp^3 bonded carbons to sp^2 state. This is also confirmed by the increase in the sp^2 content from the aromatic C=C/C–C peak at 284.6 eV to the peaks associated with different oxygen functional groups at 286.1, 287.5, and 289.2 eV, respectively. While annealing increased the concentration of sp^2 carbon, it appeared that the carbon atoms at the defect sites were highly unstable and actively captured oxygen from the environment at room temperature if exposed to the air. Interestingly, hydrogenation retained the improved sp^2 C content gained in annealing in which some sp^3 C atoms were removed. The three oxygen groups were effectively reduced through the combination of annealing/hydrogenation, especially when compared with GNPs sample which was vacuum annealed then exposed to air. C–O/C–O–C and O–C=O were kept at very low level even if the sample was allowed to contact with the air after hydrogenation, which is consistent with the overall oxygen content in Table 1. However, the sp^2 fraction is not very high because the size of graphene nanosheets in this study was very small (around 500 nm). Mattevi et al. [14] reported that an sp^2 fraction of about 85% for reduced GO could substantially improve electrical conductivity approaching that of pristine graphene. Our opinion is that it also depends on the size of graphene under investigation. Smaller platelets obviously possess more defect sites.

Thermogravimetric analysis (TGA) in Figure 6 shows that the reduced sample displays enhanced thermal stability with more than 98% weight retention up to at least 400°C. The unreduced sample on the other hand showed more than 10% weight loss near 400°C. The increasing stability of the reduced sample could be attributed to two factors. First, the vacuum annealing treatment at 550°C for 30 minutes could remove residual amorphous carbon from the sample. Second, replacing the edge oxygen content such as the keto or carboxylic acid functional group with increasing sp^2 fraction
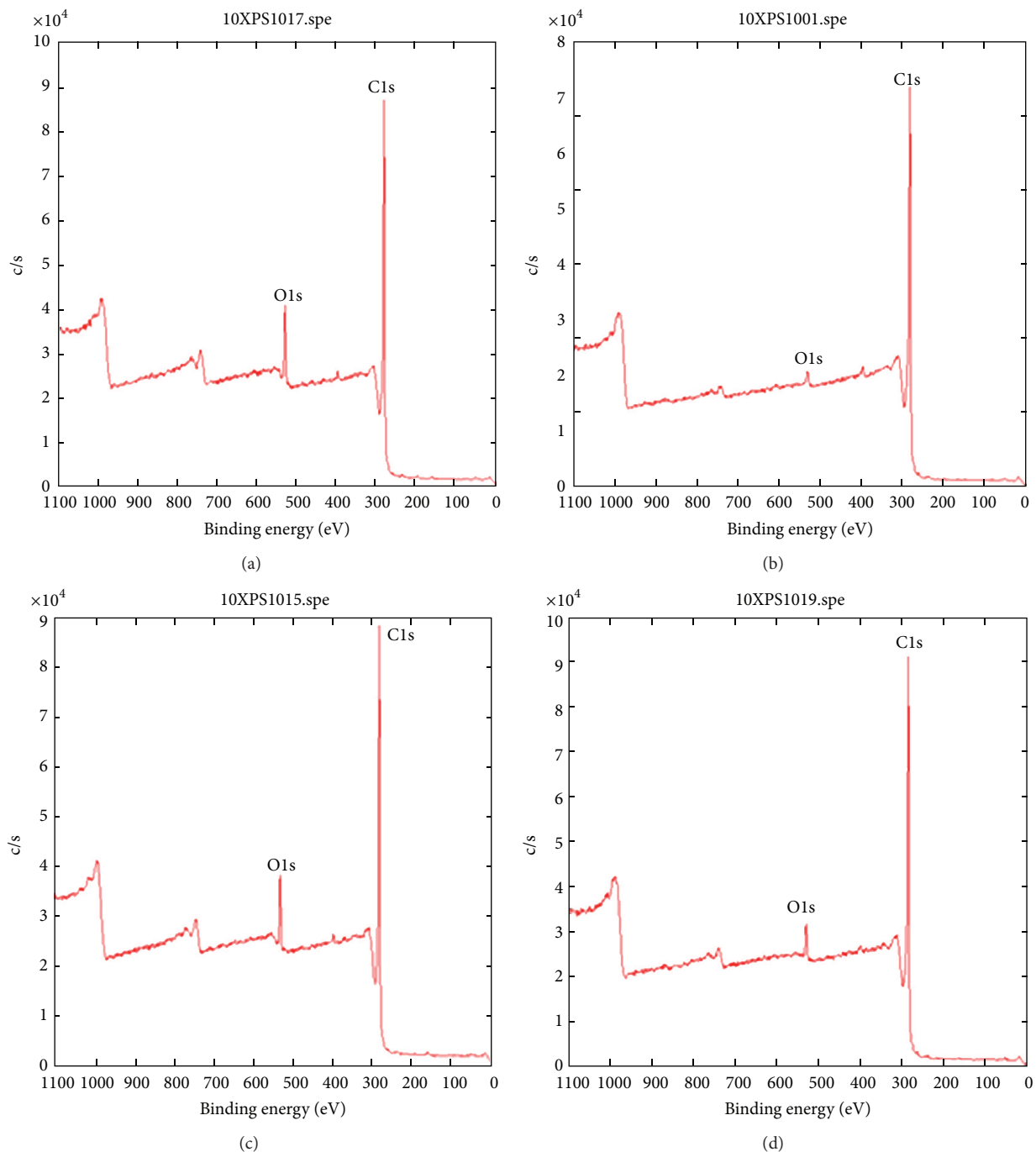
Figure 3: XPS elemental scan of GNPs. (a) GNPs; (b) GNPs annealed without exposure to air; (c) GNPs annealed then exposed to air; (d) GNPs annealed then hydrogenated.
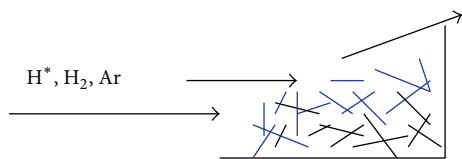

Figure 4: GNPs reduction treatment under continuous flow of Hydrogen/argon.

at the edges imparted higher thermal stability without the generation of decomposition products like CO or CO_2 [25, 26].

Typical Raman spectra for GNP and GNP-H are compared in Figure 7, and the results are summarized in Table 3. No pronounced shift in positions of D-band peak and G-band peak indicates that the two-step treatment did not cause damage to the aromatic character of these nanosheets. It is well documented that the intensity ratio of the G-band
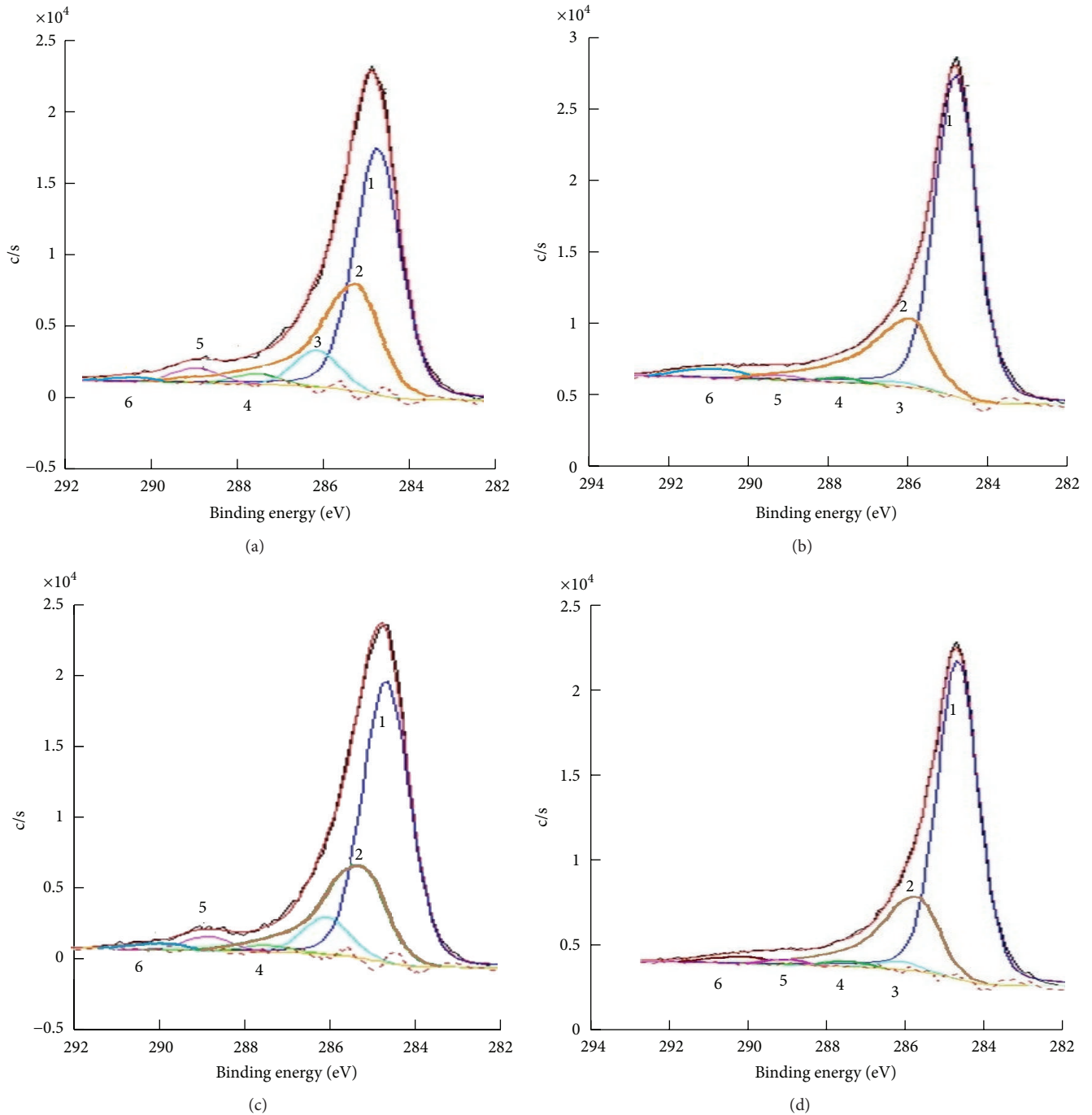
(a)

(b)

(c)

(d)

Figure 5: The C1s peaks in the XPS spectra of GNPs. (a) GNP; (b) GNP annealed without exposure to air; (c) GNP annealed then exposed to air; (d) GNP annealed then hydrogenated.

peak to the defect or disorder oriented D-band peak is an indication about the aromatic purity of the graphene basal plane [27, 28]. Even for the pure graphitic sample, the D-band is expected to be present from the termination of aromatic continuity of the basal plane by the sp^3 hybridized edge area with the presence of oxygen functional groups [27, 28]. In our study, the small increase in the G-band to the "defect and disorder" D-band intensity ratio for the reduced sample as compared to the unreduced sample indicates the

removal of amorphous carbon during the vacuum annealing treatment.

A decrease in the sheet resistance is expected with the reduction of nanosheets as reported in the literature [10, 12]. The measured surface resistance was 7.28 kohm/sq for GNPs and 3.56 kohm/sq for the reduced GNP-H, indicating almost 50% decrease in the surface resistance. There might be three mechanisms responsible for the improved conductivity: (1) in-plane conductivity of individual GNPs was increased

TABLE 2: The C1s peak position and the relative atomic percentage of various functional groups, corresponding to the deconvoluted peaks in Figure 5.

Material	C1s subpeak binding energy (eV) (bond-allocated carbon concentration (atomic%))					
	1	2	3	4	5	6
	sp^2 C	sp^3 C	C–O/C–O–C	C=O	O–C=O	π-π^*
GNP	284.68 (53.87)	285.22 (32.75)	286.18 (7.14)	287.68 (2.01)	289.18 (2.93)	290.67 (1.30)
GNP annealed, no exposure to air	284.79 (69.44)	285.95 (24.83)	286.29 (0.81)	287.79 (0.88)	289.29 (0.98)	290.83 (3.06)
GNP annealed then exposed to air	284.78 (59.23)	285.45 (27.79)	286.28 (7.25)	287.78 (1.29)	289.28 (2.76)	290.53 (1.67)
GNP-H	284.74 (69.63)	285.80 (24.51)	286.24 (1.61)	287.74 (1.05)	289.24 (1.05)	290.39 (2.16)

TABLE 3: Raman spectroscopy results for treated and untreated samples.

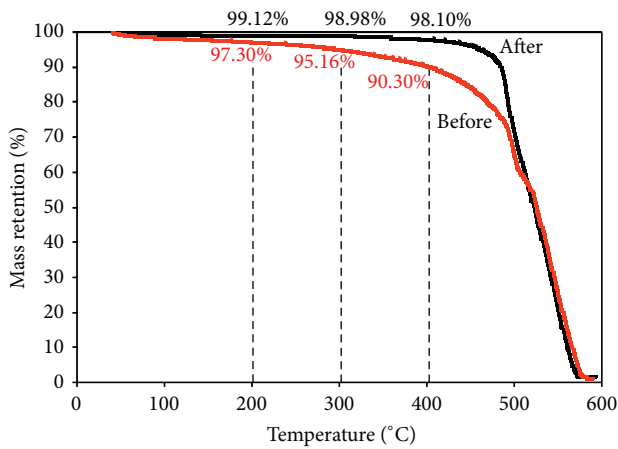| Sample	D-band peak position (1/cm)	G-band peak position (1/cm)	Intensity D/G (%)
GNP	1338.6 ± 1.7	1568.2 ± 1.2	41 ± 3.5
GNP annealed then exposed to air	1337.4 ± 3.8	1567.1 ± 1.2	42 ± 6.1
GNP-H	1338.1 ± 3.6	1567.2 ± 1.2	36 ± 8.7

FIGURE 6: Thermogravimetric analysis of GNPs before and after annealing/hydrogenation.
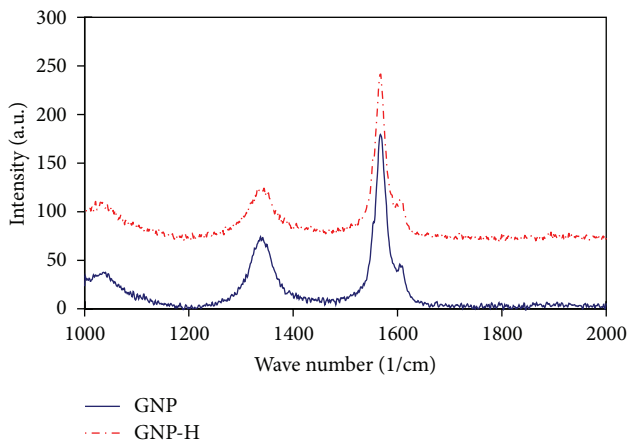

FIGURE 7: Raman spectroscopy spectra of unreduced (GNP) and reduced GNPs (GNP-H).

by the generation of larger fraction of sp^2 carbon upon reduction, (2) there were fewer oxygen groups at the defect sites to bind electrons moving in GNPs plane, (3) fewer large oxygen functional groups anchored at the defect sites led to less distortion of the GNP packing such that the transport of electrons among graphene nanosheets was enhanced. In our investigation, oxygen functional groups, primarily present at the edges of GNPs, functioned as an insulator to impede the transport of electrons among graphene nanosheets. The replacement of oxygen groups with hydrogen atoms at least had some role to play in the above mechanisms (2) and (3) because hydrogen is less electronegative than oxygen and the size of hydrogen atom is much smaller than that of an oxygen group. It is evident from Table 2 that the increased sp^2 carbon content also contributed to a better electrical conductivity. Note that the reduction in electrical resistance was 51%, not in magnitude which is seen normally for reduced GO [17]. The reason is that GO has less than 15 atomic% sp^2 carbon [17]; therefore, there is substantial improvement in electrical conductivity upon reduction treatment of GO. However, reduced GO cannot out-perform the pristine graphene nanosheets [14], whereas our two-step treated graphenes further doubled the electrical conductivity compared with the pristine graphene.

The potential-dependent capacitance characteristics of the electrodes prepared from small nanosheets in the reduced and unreduced state was determined to investigate the effect of the oxygen functional groups at the edges. The typical potential capacitance characteristics for large area graphene basal plane exhibit a linear increase on both sides of the potential of zero charge (PZC) as reported earlier for the basal plane of highly oriented pyrolytic graphite [29–32].

As shown in Figure 8(a), the small unreduced GNPs exhibited much higher capacitance and a complex potential dependence of capacitance over the same potential range. This could be the results of the effect of increased surface area, porosity, and the edge oxygen functional groups resulting
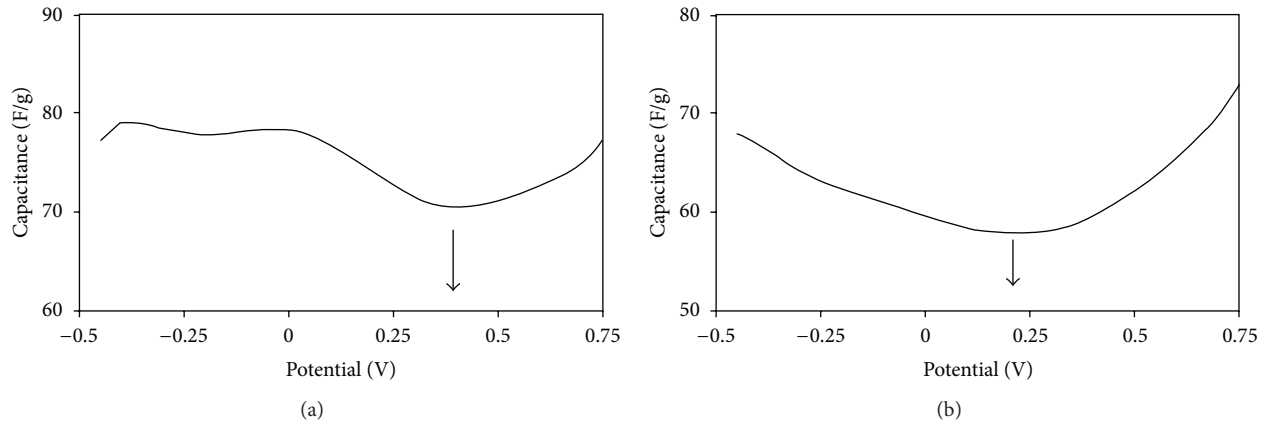
FIGURE 8: Potential capacitance characteristics. Capacitance measured at different applied potential in 0.1 M NaF aqueous solution for different materials, (a) unreduced, (b) reduced GNPs.

from going from large to small nanosheets [14, 29–32]. The oxygen functional groups contribute to the increasing capacitance from the reversible change in the oxidation-reduction state with the solvated electrolyte ions [32]. The complex potential capacitance behavior also originated from the changing oxidation state at different potentials. The occurrence of the broad and nearly flat band potential capacitance characteristics for the unreduced GNPs was possibly a result of the redistribution of charges in the presence of surface functional groups at the edges as compared to the larger and inert basal plane area for the larger graphene nanosheets [32].

After reduction, the specific capacitance decreased as compared to the unreduced state. Interestingly, the complex potential capacitance relation recovered the parabolic characteristics with a broad potential minimum near the PZC as shown in Figure 8(b). A decrease in the specific capacitance is expected from the reduced contribution to the capacitance from the reduction of oxygen functional groups [14, 29–32]. The reductive process also led to the recovery of parabolic shape of the response curve implying greater graphitic characteristics of the system. However, the clear shift in the potential minima away from the PZC was possibly due to the contribution of remaining surface active oxygen functional groups as was found for the larger nanosheets.

From the above results, we conclude that the presence of oxygen functional groups at the edges of GNPs affects the potential capacitance characteristics and the specific capacitance of the electrode. With reduction, the specific capacitance decreases, and the parabolic potential capacitance characteristics are recovered.

The electrochemical stabilities of the electrodes were compared in a two-electrode configuration for the unreduced and the reduced GNPs. Without the addition of any binder material, the dispersion of nanosheets was stirred overnight in isopropanol, and the slurry was then evenly spread on a stainless steel current collector and dried at 80°C under vacuum to remove any remaining solvent. The electrodes were then assembled with a cellulose paper separator in a two-electrode configuration which was tightened and

immersed in 6 M aqueous KOH solution for electrochemical characterization. A galvanostatic constant current technique was used to characterize the charge-discharge characteristics of these electrodes at 1 A/g discharge current density.

As shown in Figures 9(a) and 9(b), the control sample exhibited a voltage drop (IR drop) of ~200 mv at the vertex potential during the discharge cycle. The voltage drop remained almost constant with increasing discharge cycle number from the 50th to 1000th cycles. As shown in Figures 9(c) and 9(d), for the hydrogenated sample, the initial voltage drop was close to 200 mv, which decreased to 75 mv with increasing cycle number from 50th to 1000th cycle. For the hydrogenated sample, this could be explained by the nanosheet wettability. With the reduction of oxygen functional groups, the hydrophobicity of the small graphene nanosheets increased and thereby reducing the wettability of the electrode to limit the ease of aqueous electrolytic diffusion to the mesoporous network inside the bulk electrode. With increasing electrochemical cycles, the electrode wettability improved to reduce the voltage drop from 200 to 75 mv. Thus, the rate capability for the hydrogenated electrode was enhanced with increasing cycle number. The higher electrical conductivity of the hydrogenated GNPs could also be another factor for better rate capability of the electrode.

4. Summary and Conclusion

In this investigation, small graphene nanosheets with a high edge oxygen concentration were vacuum annealed (550°C) and hydrogenated (150–200°C) to reduce the atomic oxygen content from 9.5 to 4.8 atomic%. Exposure of the vacuum annealed sample to air was found to be responsible for the spontaneous repopulation of the edge sites upon exposure to atmospheric oxygen. Hydrogenation of the vacuum annealed sample is therefore essential to keep the active edge sites largely immune from the recombination with atmospheric oxygen. XPS analysis clearly revealed an equivalent increase in the sp^2 content of the reduced sample from the unreduced state in which the oxygen functional groups were present
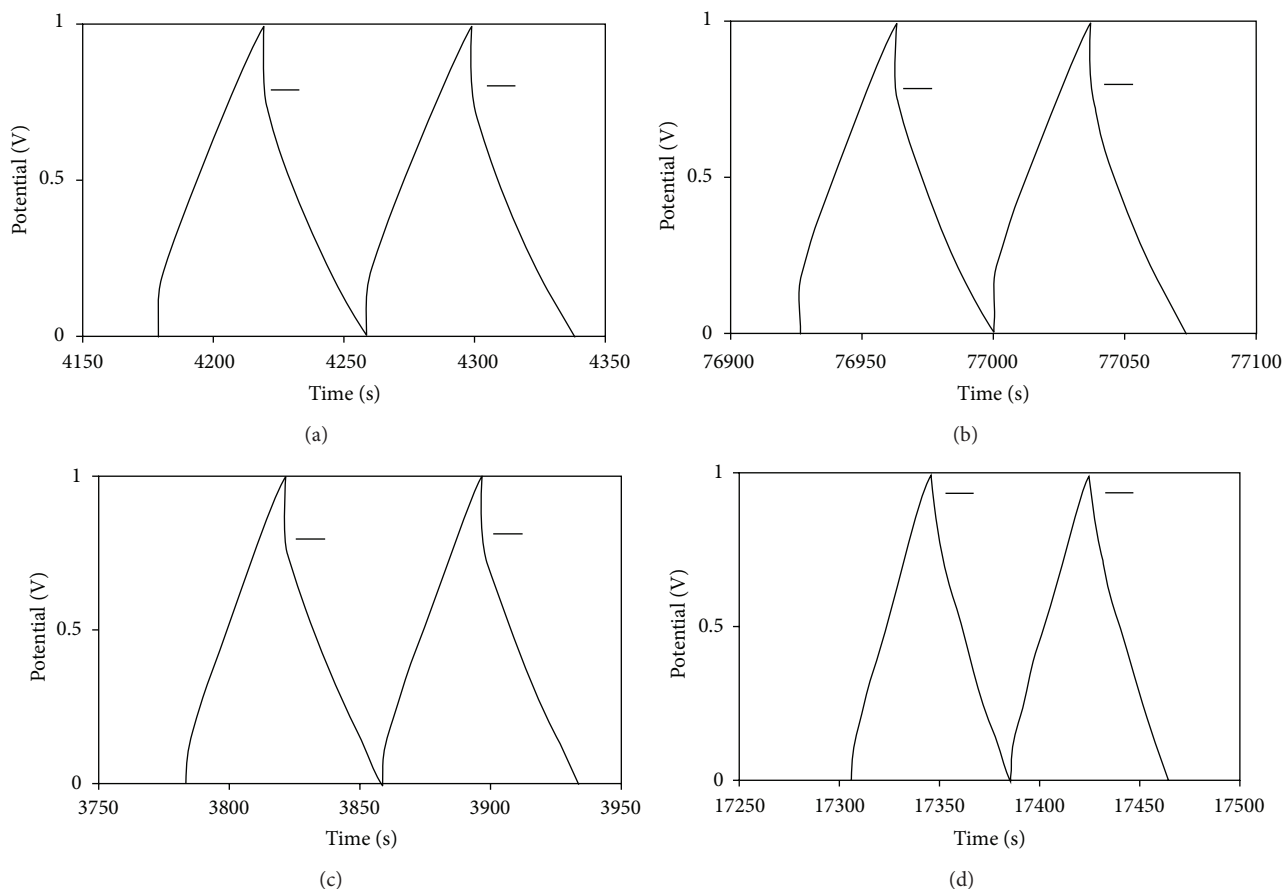
FIGURE 9: Constant current charge discharge characteristics of GNPs-based electrodes at 1 A/g discharge current density. ((a), (b)) charge-discharge characteristics of unreduced GNPs at 50th and 1000th cycles and ((c), (d)) charge-discharge characteristics of reduced GNPs at 50th and 1000th cycles.

before the two-step reduction process. The hydrogenated sample was thermally, stable and the surface resistance decreased by almost 50% as a result of the reduced edge to edge interparticle resistance due to the reduction of oxygen functional groups. The decrease in edge oxygen content was also evidenced by the recovery of parabolic potential capacitance characteristics for the hydrogenated sample as compared to the unreduced sample. The unreduced sample on the other hand exhibited a complex potential capacitance relation from the reversible oxidation-reduction process associated with the oxygen functional groups primarily present at the edge defect sites. The hydrogenated sample demonstrated better stability with increasing electrochemical cycles for electrochemical capacitor applications.

Acknowledgments

References

[1] A. K. Geim and K. S. Novoselov, "The rise of graphene," *Nature Materials*, vol. 6, no. 3, pp. 183–191, 2007.

[2] M. J. Allen, V. C. Tung, and R. B. Kaner, "Honeycomb carbon: a review of graphene," *Chemical Reviews*, vol. 110, no. 1, pp. 132–145, 2010.

[3] C. N. R. Rao, A. K. Sood, K. S. Subrahmanyam, and A. Govindaraj, "Graphene: the new two-dimensional nanomaterial," *Angewandte Chemie*, vol. 48, no. 42, pp. 7752–7777, 2009.

[4] A. K. Geim, "Graphene: status and prospects," *Science*, vol. 324, no. 5934, pp. 1530–1534, 2009.

[5] J. H. Warner, F. Schäffel, M. H. Rümmeli, and B. Büchner, "Examining the edges of multi-layer graphene sheets," *Chemistry of Materials*, vol. 21, no. 12, pp. 2418–2421, 2009.

[6] T. Enoki, Y. Kobayashi, and K.-I. Fukui, "Electronic structures of graphene edges and nanographene," *International Reviews in Physical Chemistry*, vol. 26, no. 4, pp. 609–645, 2007.

[7] H. Fukushima, *Graphite reinforcements in polymer nanocomposites [Ph.D. thesis]*, Department of Chemical Engineering and Materials Science, Michigan State University, East Lansing, Mich, USA, 2003.

[8] S. Biswas and L. T. Drzal, "Multilayered nano-architecture of variable sized graphene nanosheets for enhanced supercapacitor electrode performance," *ACS Applied Materials and Interfaces*, vol. 2, no. 8, pp. 2293–2300, 2010.

[9] S. Biswas and L. T. Drzal, "Multilayered nanoarchitecture of graphene nanosheets and polypyrrole nanowires for high performance supercapacitor electrodes," *Chemistry of Materials*, vol. 22, no. 20, pp. 5667–5671, 2010.

[10] S. Mitra and S. Sampath, "Electrochemical capacitors based on exfoliated graphite electrodes," *Electrochemical and Solid-State Letters*, vol. 7, no. 9, pp. A264–A268, 2004.

[11] M. D. Stoller, S. Park, Z. Yanwu, J. An, and R. S. Ruoff, "Graphene-based ultracapacitors," *Nano Letters*, vol. 8, no. 10, pp. 3498–3502, 2008.

[12] E. Conway, *Electrochemical Supercapacitors: Scientific Fundamentals and Technological Applications*, Plenum, New York, NY, USA, 1st edition, 1999.

[13] G. Lota, T. A. Centeno, E. Frackowiak, and F. Stoeckli, "Improvement of the structural and chemical properties of a commercial activated carbon for its application in electrochemical capacitors," *Electrochimica Acta*, vol. 53, no. 5, pp. 2210–2216, 2008.

[14] C. Mattevi, G. Eda, S. Agnoli et al., "Evolution of electrical, chemical, and structural properties of transparent and conducting chemically derived graphene thin films," *Advanced Functional Materials*, vol. 19, no. 16, pp. 2577–2583, 2009.

[15] V. C. Tung, M. J. Allen, Y. Yang, and R. B. Kaner, "High-throughput solution processing of large-scale graphene," *Nature Nanotechnology*, vol. 4, no. 1, pp. 25–29, 2009.

[16] S. Stankovich, D. A. Dikin, R. D. Piner et al., "Synthesis of graphene-based nanosheets via chemical reduction of exfoliated graphite oxide," *Carbon*, vol. 45, no. 7, pp. 1558–1565, 2007.

[17] H.-J. Shin, K. K. Kim, A. Benayad et al., "Efficient reduction of graphite oxide by sodium borohydride and its effect on electrical conductance," *Advanced Functional Materials*, vol. 19, no. 12, pp. 1987–1992, 2009.

[18] A. B. Bourlinos, D. Gournis, D. Petridis, T. Szabó, A. Szeri, and I. Dékány, "Graphite oxide: chemical reduction to graphite and surface modification with primary aliphatic amines and amino acids," *Langmuir*, vol. 19, no. 15, pp. 6050–6055, 2003.

[19] S. Park and R. S. Ruoff, "Chemical methods for the production of graphenes," *Nature Nanotechnology*, vol. 4, no. 4, pp. 217–224, 2009.

[20] O. Akhavan, "The effect of heat treatment on formation of graphene thin films from graphene oxide nanosheets," *Carbon*, vol. 48, no. 2, pp. 509–519, 2010.

[21] K. Ihm, T.-H. Kang, D. H. Lee et al., "Oxygen contaminants affecting on the electronic structures of the carbon nano tubes grown by rapid thermal chemical vapor deposition," *Surface Science*, vol. 600, no. 18, pp. 3729–3733, 2006.

[22] A. Dinger, C. Lutterloh, J. Biener, and J. Küppers, "Hydrogen atom reactions with graphite island edges on Pt(111) surfaces: hydrogenation through Eley-Rideal and hot-atom processes," *Surface Science*, vol. 421, no. 1-2, pp. 17–26, 1999.

[23] D.-Q. Yang and E. Sacher, "Carbon is X-ray photoemission line shape analysis of highly oriented pyrolytic graphite: the influence of structural damage on peak asymmetry," *Langmuir*, vol. 22, no. 3, pp. 860–862, 2006.

[24] J. Filik, P. W. May, S. R. J. Pearce, R. K. Wild, and K. R. Hallam, "XPS and laser Raman analysis of hydrogenated amorphous carbon films," *Diamond and Related Materials*, vol. 12, no. 3–7, pp. 974–978, 2003.

[25] D. R. Dreyer, S. Park, C. W. Bielawski, and R. S. Ruoff, "The chemistry of graphene oxide," *Chemical Society Reviews*, vol. 39, no. 1, pp. 228–240, 2010.

[26] S. Park, J. An, R. D. Piner et al., "Aqueous suspension and characterization of chemically modified graphene sheets," *Chemistry of Materials*, vol. 20, no. 21, pp. 6592–6594, 2008.

[27] I. Calizo, A. A. Balandin, W. Bao, F. Miao, and C. N. Lau, "Temperature dependence of the raman spectra of graphene and graphene multilayers," *Nano Letters*, vol. 7, no. 9, pp. 2645–2649, 2007.

[28] K. N. Kudin, B. Ozbas, H. C. Schniepp, R. K. Prud'homme, I. A. Aksay, and R. Car, "Raman spectra of graphite oxide and functionalized graphene sheets," *Nano Letters*, vol. 8, no. 1, pp. 36–41, 2008.

[29] J. N. Barisci, G. G. Wallace, D. Chattopadhyay, F. Papadimitrakopoulos, and R. H. Baughman, "Electrochemical properties of single-wall carbon nanotube electrodes," *Journal of the Electrochemical Society*, vol. 150, no. 9, pp. E409–E415, 2003.

[30] J. Xia, F. Chen, J. Li, and N. Tao, "Measurement of the quantum capacitance of graphene," *Nature Nanotechnology*, vol. 4, no. 8, pp. 505–509, 2009.

[31] J.-P. Randin and E. Yeager, "Differential capacitance study on the basal plane of stress-annealed pyrolytic graphite," *Journal of Electroanalytical Chemistry*, vol. 36, no. 2, pp. 257–276, 1972.

[32] J.-P. Randin and E. Yeager, "Differential capacitance study on the edge orientation of pyrolytic graphite and glassy carbon electrodes," *Journal of Electroanalytical Chemistry*, vol. 58, no. 2, pp. 313–322, 1975.